Original Article

Quantitative energy spectrum CT in differential diagnosis of aldosterone-producing adenoma and cortisol-producing adenoma

Zhizhen Li[1], Yunjin Chen[2], Yifan Zhang[2], Jiajia Shi[2], Yamin Wan[2]

[1]Department of Endocrinology, The First Affiliated Hospital of Zhengzhou University, Zhengzhou, China; [2]Department of Radiology, The First Affiliated Hospital of Zhengzhou University, Zhengzhou, China

Contributions: (I) Conception and design: Y Wan, Z Li; (II) Administrative support: Y Wan, Z Li; (III) Provision of study materials or patients: Y Wan; (IV) Collection and assembly of data: Y Chen, Y Zhang, J Shi; (V) Data analysis and interpretation: Z Li; (VI) Manuscript writing: All authors; (VII) Final approval of manuscript: All authors.

Correspondence to: Yamin Wan, MD. Department of Radiology, The First Affiliated Hospital of Zhengzhou University, No. 1 East Jianshe Road, Zhengzhou 450052, China. Email: wanyamin@zzu.edu.cn.

Background: Patients with aldosterone-producing adenoma (APA) and cortisol-producing adenoma (CPA) show some similar clinical symptoms, and a large overlap of conventional imaging manifestations, which make the differentiation difficult. The purpose of our study was to explore the value of gemstone spectral imaging (GSI) dual-energy computed tomography (DECT) in differential diagnosis of APA and CPA, screen out meaningful energy spectral indicators and provide theoretical basis for the differential diagnosis of the two.

Methods: We retrospectively analyzed the imaging and clinical data of 30 patients with APA and 27 patients with CPA who underwent GSI DECT in The First Affiliated Hospital of Zhengzhou University (a tertiary care institution). Patients were consecutively enrolled in this study, and the quantitative DECT parameters were compared between the APA and CPA groups by two-sample test. The diagnostic efficacies were evaluated by receiver operating characteristic (ROC) analysis.

Results: DECT parameters including CT (computed tomography) values at 40–70 keV in the arterial phase, concentrations of I (H_2O) and fat (I) in the arterial phase, and the effective atomic number in the venous phase, were significantly different between the APA and CPA groups (all $P<0.001$), and the area under the curve (AUC) values are 0.80, 0.79, 0.88, 0.76, 0.82, 0.87, and 0.86.

Conclusions: DECT quantitative parameters can effectively identify APA and CPA, the CT values at 40 and 60 keV in the arterial phase, the normalized CT value at 60 keV, the I (H_2O), fat (I) concentration in the arterial phase and the effective atomic number parameter in the venous phase had valuable diagnostic performance.

Keywords: Adrenal; adenoma; spectral imaging; computed tomography (CT)

Submitted Nov 18, 2022. Accepted for publication May 15, 2023. Published online May 31, 2023.
doi: 10.21037/qims-22-1279
View this article at: https://dx.doi.org/10.21037/qims-22-1279

Introduction

Adrenal cortical adenoma (ACA) is the most common benign adrenal tumor, accounting for 50–80% of all adrenal tumors. According to whether it has secretory function, ACA can be categorized into functional ACA and non-functional ACA (1). While most non-functional ACA does not require treatment, functional ACA seriously affects the physical and mental health of patients due to the abnormal secretion of certain hormones, and usually requires active clinical intervention. The most common subtypes of functional ACA are aldosterone-producing adenoma (APA) and cortisol-producing adenoma (CPA). Treatment

strategies for APA and CPA are distinct. In terms of surgical treatment, CPA is adenomectomy on the diseased side, while APA is complete adrenalectomy on the diseased side, thus requiring an accurate differential diagnosis to guide the clinical treatment plan (2). However, patients with APA or CPA show some similar clinical symptoms and a large overlap of conventional imaging manifestations, which make the differentiation difficult. Although percutaneous cannulation of the adrenal vein sampling (AVS) is the "gold standard" for APA diagnosis, the difficulty, cost and invasiveness of the procedure limit its widespread use in clinical practice. In traditional imaging examinations, the evaluation is mainly based on the size, density, border and enhancement degree of the tumor, helping radiologists and clinicians distinguish whether adrenal masses are adenomas or non-adenomas. Further differentiating the function of ACA as APA or CPA is not available (3).

As an imaging technology, dual-energy computed tomography (DECT) or called spectrum CT has the advantages of providing multiple quantitative information for various materials inside the tissue (4), to clarify benign and malignant tumors (5,6). DECT can provide richer qualitative and quantitative diagnostic information by taking the advantage of covering a wider spectrum of energy parameters to reflect the state of blood supply and angiogenesis in a lesion directly and accurately. So far, to our best knowledge, there is barely relevant report on differentiating APA from CPA using this imaging modality. The purpose of our study is to explore the differences in energy spectral parameters between APA and CPA, screen out meaningful energy spectral indicators, and provide theoretical basis for the differential diagnosis of the two. We present this article in accordance with the STARD reporting checklist (available at https://qims.amegroups.com/article/view/10.21037/qims-22-1279/rc).

Methods

Patients

This study is a retrospective analysis of the imaging and clinical data of APA and CAP patients who underwent GSI DECT in the First Affiliated Hospital of Zhengzhou University from October 2018 to December 2020. The study was conducted according to the Declaration of Helsinki (as revised in 2013) and was approved by the Ethics Committee of The First Affiliated Hospital of Zhengzhou University. Individual consent for this retrospective analysis was waived. A total of 146 patients who were suspected of having an adrenal mass were consecutively collected. All patients underwent contrast-enhanced CT two weeks before surgery. All patients with APA performed AVS, and low-dose dexamethasone suppression tests were negative. All patients with CPA performed a low-dose dexamethasone suppression test. Inclusion criteria: (I) patients with pathologically diagnosed APA or CPA; (II) patients without any treatment before the DECT examination; (III) complete DECT data, and the image quality meets the diagnostic and post-processing standards. Exclusion criteria: (I) patients with iodine allergy, lactation, pregnancy, and major acute or chronic diseases who cannot undergo CT examination (n=32); (II) patients with incomplete data (n=27); (III) no adrenal gland lesions (n=30). After screening by the inclusion and exclusion criteria, a total of 57 patients were included in the two groups: APA group (n=30) and CPA group (n=27) (*Figure 1*).

DECT examination

Patients were in the supine position, and the CT scanning range was from the top of the liver to the lower poles of both kidneys. A GE Revolution CT machine was used to perform a plain and dual-phase enhanced scan of the abdomen. With the application of abdominal GSI scanning sequence, firstly, conventional CT scan was performed, and iodine contrast agent was injected through the cubital vein. The total amount of contrast agent used (mL) =450 mgI/kg × body weight (kg)/contrast agent concentration (mgI/mL), and the total amount of contrast agent injection was controlled within 30 s, that is, flow rate (mL/s) = contrast total dose (mL)/30 s. The arterial phase energy spectrum scan adopted an automatic triggering technology. Spectral parameters: detector width: 80 mm, pitch: 0.992:1, rotational speed: 0.5 s/r, GSI mode in arteriovenous phase, automatic mA selection; FOV: 50 cm × 50 cm; scanning slice spacing and slice thickness: 5 mm. In terms of layer spacing and layer thickness of reconstructed images, both are 1.25 mm.

Image analysis

The original data were reorganized into an image set with a slice thickness of 1.25 mm using the single-energy recombination algorithm and uploaded to the GE post-processing workstation ADW4.7 for tumor measurement, analysis and evaluation. In processing of conventional CT

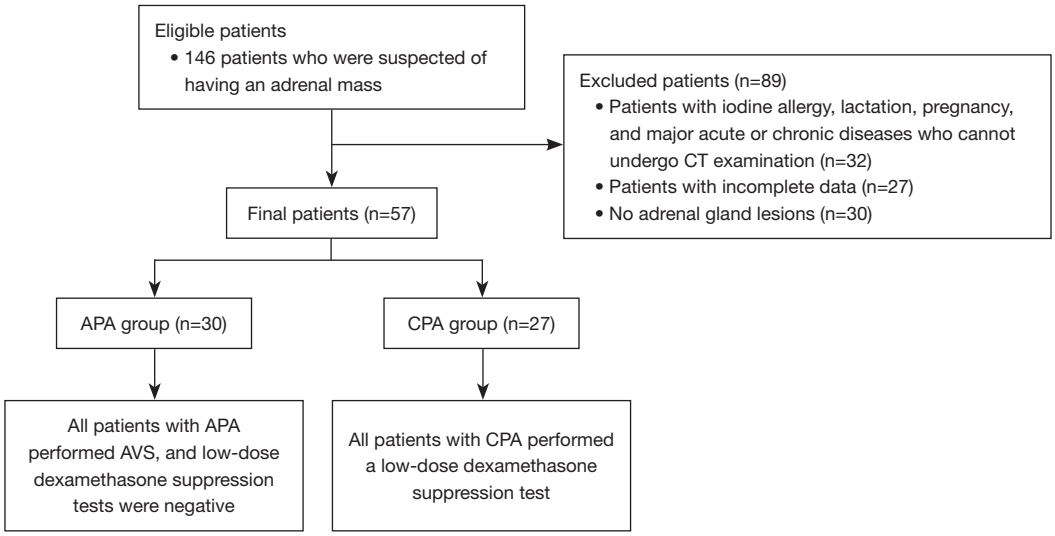

Figure 1 Flow chart of the patient recruitment with inclusion and exclusion criteria. CT, computed tomography; APA, aldosterone-producing adenoma; CPA, cortisol-producing adenoma; AVS, adrenal vein sampling.

data, the laterality of the mass, the presence or absence of calcification, cystic degeneration and other special signs were recorded; the maximum left-right diameter, maximum anterior-posterior diameter of the mass, and the average plain scan density of the mass were measured. Gemstone spectral imaging (GSI) viewer software was used to perform post-processing operations on the arterial and venous phase energy spectrum data, including adjusting the appropriate field of view, and delineating the region of interest a (ROIa) within the lesions. After the delineation was completed, another ROIb was placed at the same level in the aorta. When drawing the ROI, 1/2 to 2/3 of the slice area were covered, and the area with uniform tumor density was selected as much as possible, avoiding the tumor edge, visible blood vessels and cystic necrosis areas, and ensuring that the ROI at different phases and slices was kept same for the location, size and shape. The energy spectrum data were then exported by selecting administration → Command Window → Prefs → GSI Viewer → roiSave, and the CT values at every 10 keV interval, effective atomic numbers of different single energy levels at 40–140 keV in each arterial and venous phase, and the concentration of each pair of base substances were obtained. Since most of the energy spectrum studies (5,6) have shown that the CT value at the high keV energy level (110–140 keV) is not very different, this study only intercepted the CT value of a single energy at the 40–110 keV energy level. The energy spectrum curve was drawn according to the attenuation values at each energy level of the two phases, the slope of the energy spectrum curve of each phase and the calculated standardized energy spectrum data were obtained. The calculation formula of energy spectrum curve slope and normalized energy spectrum data are as follows: energy spectrum curve slope = (CT value 40 keV – CT value 110 keV)/(110–40); normalized energy spectrum data = ROIa data at the adrenal lesion/main layer of the same layer ROIb data at the artery. The above quantitative data were averaged from three consecutive measurements; The CT findings were evaluated by two radiologists who had 10 and 7 years of experience in abdominal radiology. Reviewers were blinded to the pathologic findings, and any disagreements were resolved by consensus after consultation with a third radiologist who had 25 years of experience in abdominal imaging.

Statistical analysis

Statistical software SPSS 23.0 (SPSS Inc., Chicago, IL, USA) was used, and the quantitative data were described in the form of mean ± standard deviation if they conformed to normal distribution. Data that conformed to normal distribution were compared by independent sample *t*-test, data that did not follow the normal distribution were compared by Mann-Whitney test. Significant indicators screened out from the comparisons between the APA and CPA groups were used to draw the receiver operating

Table 1 Comparison of the general clinical data of the APA and CPA patients

Variables	APA group	CPA group	P value
Weight (kg)	64.90±11.06	69.48±12.08	0.530
Age (years)	51.80±9.70	53.34±7.43	0.385
Diameter left-right (mm)	13.10±3.00	18.61±4.45	<0.001
Diameter front-rear (mm)	14.81±4.39	21.00±5.79	<0.001
Plain CT value	11.93±8.67	27.56±10.52	<0.001
Sex			0.536
Male	12 [40]	13 [48.1]	
Female	18 [60]	14 [51.9]	

Data are presented as mean ± standard deviation and number [frequency]. APA, aldosterone-producing adenoma; CPA, cortisol-producing adenoma; CT, computed tomography.

Table 2 CT values of two groups in arterial phase at different energy levels

Energy level (keV)	APA group (HU)	CPA group (HU)	P value
40	149.03±26.87	180.57±27.63	<0.001
50	106.00±22.04	130.81±19.89	<0.001
60	67.74±12.55	90.31±16.03	<0.001
70	50.66±13.65	64.41±12.78	<0.001
80	45.27±11.90	51.40±10.99	0.049
90	40.03±10.46	44.70±9.83	0.150
100	35.35±9.35	40.41±9.70	0.086
110	30.31±8.26	34.81±9.69	0.122

Data are presented as mean ± standard deviation. CT, computed tomography; APA, aldosterone-producing adenoma; CPA, cortisol-producing adenoma; HU, Hounsfield unit.

characteristic (ROC) curve, the area under the curve (AUC) was obtained. Such data were imported into Excel software, the Youden index was obtained according to the formula. Finally, the optimal critical value was screened out, and the sensitivity and specificity were set as the test level of 0.05.

Results

General clinical information

A total of 57 patients with ACA were included in this study, 30 in the APA group and 27 in the CPA group. In the APA group, there were 12 males and 18 females, age ranged from 29 to 70 years old. Endocrine examination and clinical symptoms of 10 cases were typical hyperaldosteronism, 20 cases were subclinical aldosteronism. In the CPA group, there were 13 males and 14 females, age ranged from 37 to 68 years old. Endocrine examination and clinical symptoms of 7 cases were typical, 20 patients had normal endocrine examination but had typical symptoms of Cushing's syndrome. There were no statistical differences in patients' weight, age and sex between the two groups, but there were significant differences in lesion size and plain CT values (*Table 1*).

Energy spectrum CT values at each single energy level in the arterial and venous phases

As shown in *Table 2*, CT values at the 40–80 keV energy levels in arterial phase were significantly different between the APA and CPA lesions (*Figure 2*). AUC at the 60 keV energy level reached the highest as 0.88, with the Youden index of 0.66 and the best diagnostic cutoff was 69.45 HU. CT value at the 60 keV energy level showed the best diagnostic sensitivity (92.60%), while CT value at 70 keV showed the best specificity of diagnosis (79.35%) (*Table 3*). Normalized CT values in the arterial phase at different energy levels were further analyzed, and similarly the CPA lesions showed significant higher values at the 40–70 keV energy levels than the APA lesions (Table S1).

In contrast to the arterial phase, CT values at each single energy level in the venous phase were mostly not different between the APA and CPA groups, except the value at the 70 keV in APA group was significantly higher than that of

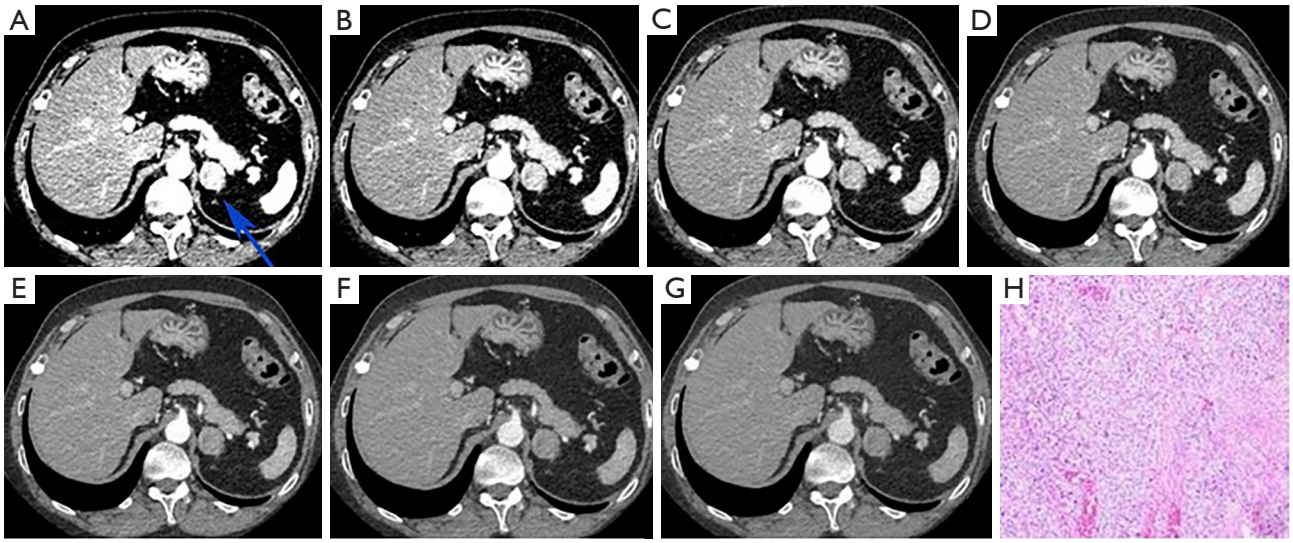

Figure 2 CT image of an arterial phase 40 keV energy level from a 48-year-old male patient with CPA lesion located in the left adrenal gland (blue arrow in A). The attenuation value of the lesion was 197.98 HU; (B) CT image of 50 keV energy level in arterial phase, with a decay value of 142.63 for lesions; (C) CT image of 60 keV energy level in arterial phase, with a lesion attenuation value of 96.34; (D) CT image of 70 keV energy level in arterial phase, lesion attenuation value of 78.56; (E) CT image of 80 keV energy level in the arterial phase, the attenuation value of the lesion is 65.87; (F) CT image of 90 keV energy level in arterial phase, with lesion attenuation value of 59.99; (G) CT image of 100 keV energy level in the arterial phase with an attenuation value of 54.59 HU for lesions. At low energy levels (40–60 keV), the attenuation values are higher, and they differ greater; the lesions are clearly displayed and have strong contrast, but the noise is high, and the fine structure is not well displayed; as the energy level increases, the noise is relatively reduced, but the image contrast is reduced. (H) The H&E-stained image of the CPA tumor section under 20× objective, showing riches of clear cells. CT, computed tomography; CPA, cortisol-producing adenoma; HU, Hounsfield unit; H&E, hematoxylin and eosin.

Table 3 ROC curve results of 40–80 keV in arterial phase of two groups

Energy level (keV)	AUC	Youden Index	Sensitivity (%)	Specificity (%)	Optimum diagnostic (HU)
40	0.80	0.51	77.80	73.30	166.24
50	0.79	0.57	81.50	70.00	117.27
60	0.88	0.66	92.60	73.30	69.45
70	0.76	0.51	74.68	79.35	56.92
80	0.67	0.32	55.60	76.70	52.62

ROC, receiver operating characteristic; AUC, area under the curve; HU, Hounsfield unit.

Table 4 CT values of two groups in venous phase at different energy levels

Energy level (keV)	APA (HU)	CPA (HU)	P value
40	171.74±20.95	159.64±26.19	0.060
50	129.12±20.27	132.46±16.59	0.784
60	105.16±19.37	100.72±15.28	0.397
70	79.44±14.73	66.83±12.20	<0.001
80	60.36±12.95	55.98±9.71	0.106
90	48.35±9.10	43.64±8.97	0.178
100	40.54±9.57	37.28±8.01	0.280
110	33.41±5.10	30.56±6.89	0.143

Data are presented as mean ± standard deviation. CT, computed tomography; APA, aldosterone-producing adenoma; CPA, cortisol-producing adenoma; HU, Hounsfield unit.

Table 5 Comparisons of concentrations of base substance pairs between two groups in arterial phase

Base substance pairs	APA group (HU)	CPA group (HU)	P value
I (H_2O) (100 μg/cm^3)	18.79±2.35	21.90±2.42	<0.001
I (fat) (200 μg/cm^3)	20.15±2.63	16.40±3.91	<0.001
Fat (I) (mg/cm^3)	1,062.57±45.26	1,003.27±19.15	<0.001

Data are presented as mean ± standard deviation. APA, aldosterone-producing adenoma; CPA, cortisol-producing adenoma; HU, Hounsfield unit; H_2O, water.

the CPA group (*Table 4*). The AUC at 70 keV was 0.75, the Youden index was 0.53, the optimal diagnostic cutoff was 69.33 HU, the diagnostic sensitivity was 83.30%, and the diagnostic specificity was 71.40%. Normalized CT value at 70 keV in the venous phase was also significantly higher in the APA group than that of the CPA lesions (Table S2).

Energy spectrum parameters of each base substance pair concentration and effective atomic number in arterial and venous phases

In the arterial phase of DECT, the concentration of I (H_2O) in the CPA lesions was significantly higher than that of the APA lesions, while the CPA lesions contained significantly lower concentrations of I (fat) and fat (I) than those of APA lesions (*Table 5*). AUC and Youden index of fat (I) concentration was the highest among the three parameters (0.87 and 0.76, respectively); concentration of I (H_2O) showed the best specificity (96.70%); concentration of I (fat) showed the best sensitivity (83.30%) (*Table 6*). There was no significant difference in the effective atomic number of lesions between the two groups in the arterial phase.

As slightly different from the arterial phase, each base substance pair including concentrations of I (H_2O), I (fat) and Ca (fat) were all significantly higher in the APA than CPA lesions in the venous phases, as well as for the effective atomic number (*Table 7*). The effective atomic number showed the highest AUC, Youden index, sensitivity and

Table 6 Results of ROC curve of base substance pairs between two groups in arterial phase

Base substance pairs	AUC	Youden index	Sensitivity (%)	Specificity (%)	Optimum diagnostic (HU)
I (H_2O) (100 μg/cm^3)	0.82	0.52	55.60	96.70	21.84
I (fat) (200 μg/cm^3)	0.77	0.54	83.30	71.40	18.52
Fat (I) (mg/cm^3)	0.87	0.76	80.00	89.00	1,021.97

ROC, receiver operating characteristic; AUC, area under the curve; H_2O, water; HU, Hounsfield unit.

specificity (*Table 8*).

Discussion

Differential diagnosis of APA and CPA are clinically significant but challenging. Subclinical CPA is the most common functional adrenal tumors (7), while as many as 30% of APA patients manifest the similar clinical symptoms as CPA because of hypokalemia (8,9); which makes it particularly difficult to distinguish between the two from a clinical perspective. Furthermore, 10–20% of ACAs occur bilaterally or with multiple lesions (3,10), functional diagnosis is challenging when the responsible lesion needs to be accurately located (3,8,11). Percutaneous cannulation of the adrenal vein is the "gold standard" for APA diagnosis, but the difficulty, cost and invasiveness of the procedure limit its widespread use in clinical practice (12). Previous study (13) reported different presentations of the APA and CPA lesions by conventional CT/MRI imaging, but the difference is far beyond distinguishing them accurately. In terms of medication treatment, CPA is mostly treated with mitotane, while APA is treated with spironolactone (2). Early and accurate identification of APA or CPA from the imaging perspective is of great significance in guiding clinical treatment.

Spectral CT imaging technology shows a great potential in differentiation tumors or small lesions (14-17), by providing richer qualitative and quantitative diagnostic information, and improved signal-to-noise ratio and spatial resolution than conventional CT (18). This study provided first-hand evidence on the critical energy-spectrum CT features in differential diagnosing of APA and CPA, especially the base substance concentrations of I (H_2O), I (fat) and fat (I) in the arterial phase, and the I (H_2O), fat (I) and Ca (fat) in the venous phase. I (H_2O) concentration can reflect the state of blood supply and angiogenesis of the lesion more directly and accurately than traditional CT values (19). The I (H_2O) concentration in the arterial phase of APA was lower than that in the CPA tumors in this study, presumably due to the observations that most vessels in the APA are located in a halo-like distribution under the envelope, so there is a "paper-thin" enhancement at the edges during the enhanced arterial phase, and the central enhancement is lower than the edges (20). The fat (I) concentration was higher in the arterial APA group than in the CPA group, which is related to the higher intracellular lipid content of APA in comparing to CPA. Wan *et al.* (21) showed that iodine-lipid concentration had the highest diagnostic effect on adrenal hypolipidemia adenoma and nodular hyperplasia. The I (H_2O) and fat (I) concentrations in the intravenous phase were slightly higher in the APA group than in the CPA group, presumably because CPA often showed moderate or even significant intensification in the arterial phase and mostly receded in the intravenous phase; however, APA showed mild to moderate intensification in the arterial phase and delayed or mildly decreased intensification in the intravenous phase (22). The overall degree of venous enhancement of the adenoma was essentially the same in both groups. The difference in Ca (fat) concentration in the intravenous

Table 7 Comparisons of concentrations of base substance pairs between two groups in venous phase

Base substance pairs	APA group (HU)	CAP group (HU)	P value
I (H_2O) (100 μg/cm^3)	22.71±1.92	20.73±2.12	0.001
I (fat) (200 μg/cm^3)	21.07±2.36	18.92±1.36	<0.001
Ca (fat) (mg/cm^3)	59.25±4.03	54.31±5.47	<0.001
Effective atomic number (Z)	8.98±0.17	8.63±0.27	<0.001

Data are presented as mean ± standard deviation. APA, aldosterone-producing adenoma; CPA, cortisol-producing adenoma; H_2O, water; HU, Hounsfield unit.

Table 8 ROC curve results of base substance pairs between two groups in venous phase

Base substance pairs	AUC	Youden Index	Sensitivity (%)	Specificity (%)	Optimum diagnostic (HU)
I (H_2O) (100 μg/cm^3)	0.78	0.52	93.47	56.40	20.14
I (fat) (200 μg/cm^3)	0.79	0.62	65.43	91.86	20.99
Ca (fat) (mg/cm^3)	0.79	0.51	75.36	70.45	56.53
Effective atomic number (Z)	0.86	0.71	97.31	92.43	8.71

ROC, receiver operating characteristic; AUC, area under the curve; H_2O, water; HU, Hounsfield unit.

phase was statistically significant and may be related to the subtle differences in calcium elements within the lesion. The interaction of X-rays with a compound can be equated to the interaction with a single substance whose atomic number is called the effective atomic number (Zeff) (23). In this study, there was a statistical difference in the number of effective atomic sequences in the venous phase between the two groups (AUC of 0.86), presumably due to the difference in the content of lipid and solid components in the two groups of lesions. Each substance has a different slope of spectral curve, so the composition of the substance can be analyzed from the slope of spectral curve (24). In the present study, the arteriovenous energy spectrum curves were both descending and similar in morphology, indicating that the lesions in both groups were of the same origin. The arteriovenous energy spectrum curves of the CPA group were located above the original APA group because the enhancement in the arteriovenous phase of CPA was more obvious than that of APA. And the lower the keV, the greater the difference in slope of the energy spectrum curve, and the higher the diagnostic efficacy. These results are in general agreement with the study of Forghani *et al.* in evaluation of the soft tissues of the neck (25). These further demonstrate the pathophysiological implications of using the spectral CT imaging technology to study APA and CPA.

Lesion size and plain CT values were examined by conventional CT for both groups in our study: the average diameter of APAs was significantly smaller than that of CPAs; the average flat-scan CT value of the APAs was smaller than that of the CPAs. APA often leads to hypertension and hypokalemia, which are easily detected in the early stage of the disease because the body is more sensitive to hypokalemic response but tolerant to Cushing's syndrome by the CPAs. The difference on flat-scan CT values is related to the histocytological differences between APA and CPA. APA is rich in clear cells with large volume and uniform distribution of lipid components (17); whereas CPA consists of granular cells with small volume and dispersed distribution of lipid components. However, these conventional imaging presentations are not sufficient to differentiate the two groups. In contrast, the energy spectrum CT values at 40 and 60 keV in the arterial phase, standardized CT values at 60 keV, I (H_2O) and fat (I) concentrations in the arterial phase and effective atomic number in the venous phase were all with AUCs of 0.80 and above indicating a relatively good diagnostic efficacy. Furthermore, we conceive to construct a scoring system for future study using the imaging data in conjunction with tumor size to facilitate clinical differential diagnosis of APA/CPA.

Shortcomings of this study include: (I) this was a single-center, retrospective study, which may be with possible selection bias; (II) the sample size of lesions in both groups was small, and we would continue to collect cases and enrich the sample size in the future; (III) the difference between the energy spectrum parameters of adrenal non-functional adenoma and APA versus Cushing's adenoma was not explored.

Conclusions

We tried for the first time to use dual-energy CT to explore the pathophysiological implications on APA and CPA, in which the CT values of 40 and 60 keV in the arterial stage, the concentrations of arterial stage I (H_2O) and fat (I), and the effective atomic number in the venous phase have certain significance in the differential diagnosis of APA. In conjunction with our previous report in using spectral CT multi-parameters in differential diagnosis of lipid-poor adrenal adenoma and adrenal nodular hyperplasia and Cushing adenoma, all our data support the new idea and methods for the classification of functional adrenal adenoma by the spectral CT imaging, which can better guide clinical treatment.

Acknowledgments

Funding: This work was supported by the Science and Technology Department of Henan Province (No. 212102310802).

Footnote

Reporting Checklist: The authors have completed the STARD reporting checklist. Available at https://qims.amegroups.com/article/view/10.21037/qims-22-1279/rc

Conflicts of Interest: All authors have completed the ICMJE uniform disclosure form (available at https://qims.amegroups.com/article/view/10.21037/qims-22-1279/coif). The authors have no conflicts of interest to declare.

Ethical Statement: The authors are accountable for all aspects of the work in ensuring that questions related to the accuracy or integrity of any part of the work are appropriately investigated and resolved. The study was conducted according to the Declaration of Helsinki (as

revised in 2013) and was approved by the Ethics Committee of The First Affiliated Hospital of Zhengzhou University. Individual consent for this retrospective analysis was waived.

References

1. Elbanan MG, Javadi S, Ganeshan D, Habra MA, Rao Korivi B, Faria SC, Elsayes KM. Adrenal cortical adenoma: current update, imaging features, atypical findings, and mimics. Abdom Radiol (NY) 2020;45:905-16.
2. Dogrul AB, Cennet O, Dincer AH. Minimally invasive techniques in benign and malignant adrenal tumors. World J Clin Cases 2022;10:12812-21.
3. Alimu P, Fang C, Han Y, Dai J, Xie C, Wang J, Mao Y, Chen Y, Yao L, Lv C, Xu D, Xie G, Sun F. Artificial intelligence with a deep learning network for the quantification and distinction of functional adrenal tumors based on contrast-enhanced CT images. Quant Imaging Med Surg 2023;13:2675-87.
4. Wan Y, Hao H, Chen Y, Zhang Y, Yue Q, Li Z. Application of spectral CT combined with perfusion scan in diagnosis of pancreatic neuroendocrine tumors. Insights Imaging 2022;13:145.
5. Wan Y, Hao H, Meng S, Li Z, Yu F, Meng Chi, Chao Q, Gao J. Application of low dose pancreas perfusion CT combined with enhancement scanning in diagnosis of pancreatic neuroendocrine tumors. Pancreatology 2021;21:240-5.
6. Lan X, Wang X, Qi J, Chen H, Zeng X, Shi J, Liu D, Shen H, Zhang J. Application of machine learning with multiparametric dual-energy computed tomography of the breast to differentiate between benign and malignant lesions. Quant Imaging Med Surg 2022;12:810-22.
7. Kmieć P, Zalewska E, Kunicka K, Świerblewska E, Sworczak K. Autonomous Aldosterone Secretion in Patients with Adrenal Incidentaloma. Biomedicines 2022.
8. Miyamoto S, Yoshida Y, Ozeki Y, Okamoto M, Gotoh K, Masaki T, Nishida H, Fujinami H, Shin T, Daa T, Asayama Y, Shibata H. Pitfalls in the diagnosis and treatment of a hypertensive patient with unilateral primary aldosteronism and contralateral pheochromocytoma: a case report. BMC Endocr Disord 2023;23:44.
9. Vaidya A, Hundemer GL, Nanba K, Parksook WW, Brown JM. Primary Aldosteronism: State-of-the-Art Review. Am J Hypertens 2022;35:967-88.
10. Yalon T, Yalon M, Assaf D, Lenartowicz K, Foster T, Lyden M, Dy B, Bancos I, McKenzie T. Differentiating between adrenocortical carcinoma and lipid-poor cortical adenoma: A novel cross-sectional imaging-based score. Surgery 2023;173:35-42.
11. Balomenaki M, Margaritopoulos D, Vassiliadi DA, Tsagarakis S. Diagnostic workup of Cushing's syndrome. J Neuroendocrinol 2022;34:e13111.
12. Kumasaka S, Tokue H, Tsushima Y. Difficulty factors of adrenal venous sampling based on patient characteristics and imaging findings. Acta Radiol 2022;63:1276-82.
13. Bracci B, De Santis D, Del Gaudio A, Faugno MC, Romano A, Tarallo M, Zerunian M, Guido G, Polici M, Polidori T, Pucciarelli F, Matarazzo I, Laghi A, Caruso D. Adrenal Lesions: A Review of Imaging. Diagnostics (Basel) 2022.
14. Wen Q, Yue Y, Shang J, Lu X, Gao L, Hou Y. The application of dual-layer spectral detector computed tomography in solitary pulmonary nodule identification. Quant Imaging Med Surg 2021;11:521-32.
15. Lin GH, Chen WY, Chen CM, Cheng X, Zhou BH, Ji JS. Construction of prediction model combined dual-energy CT quantitative parameters and conventional CT features for assessing the Ki-67 expression levels in invasive breast cancer. Zhonghua Yi Xue Za Zhi 2022;102:1753-9.
16. Liang G, Yu W, Liu SQ, Xie MG, Liu M. The value of radiomics based on dual-energy CT for differentiating benign from malignant solitary pulmonary nodules. BMC Med Imaging 2022;22:95.
17. Shern Liang E, Wastney T, Dobeli K, Hacking C. Virtual non-contrast detector-based spectral CT predictably overestimates tissue density for the characterisation of adrenal lesions compared to true non-contrast CT. Abdom Radiol (NY) 2022;47:2462-7.
18. Fink MA, Seibold C, Kauczor HU, Stiefelhagen R, Kleesiek J. Jointly Optimized Deep Neural Networks to Synthesize Monoenergetic Images from Single-Energy CT Angiography for Improving Classification of Pulmonary Embolism. Diagnostics (Basel) 2022.
19. Lochschmidt ME, Gassenhuber M, Riederer I, Hammel J, Birnbacher L, Busse M, Boeckh-Behrens T, Ikenberg B,

Wunderlich S, Liesche-Starnecker F, Schlegel J, Makowski MR, Zimmer C, Pfeiffer F, Pfeiffer D. Five material tissue decomposition by dual energy computed tomography. Sci Rep 2022;12:17117.
20. McPhedran R, Gerson R, Alfaleh H, Sathiadoss P, Schieda N. Inter-individual comparison of diagnostic accuracy of adrenal washout CT compared to chemical shift MRI plus the T2-weighted (T2W) adrenal MRI calculator in indeterminate adrenal masses: a retrospective non-inferiority study. Abdom Radiol (NY) 2022;47:2453-61.
21. Wan Y, Chen Y, Yu F, Cai M, Lv D, Gao J. Spectral CT multi-parameters in diferential diagnosis of lipid-poor adrenal adenoma and adrenal nodular hyperplasia. Chinese Journal Of Medical Imaging Technology 2021;37:909-13.
22. Araujo-Castro M, Parra-Ramírez P. Diagnosis of primary hyperaldosteronism. Med Clin (Barc) 2022;158:424-30.
23. Yao C, Chen X, Yang Z, Huang R, Zhang S, Liao Y, Chen X, Dai Z. Gemstone Spectral CT Virtual Noncontrast Images and Iodine Maps for the Characterization of Thyroid Lesions and Distinguishing Thyroid Papillary Carcinoma from Nodular Goiter. Int J Endocrinol 2023;2023:8220034.
24. Greffier J, Villani N, Defez D, Dabli D, Si-Mohamed S. Spectral CT imaging: Technical principles of dual-energy CT and multi-energy photon-counting CT. Diagn Interv Imaging 2023;104:167-77.
25. Forghani R, Mukherji SK. Advanced dual-energy CT applications for the evaluation of the soft tissues of the neck. Clin Radiol 2018;73:70-80.

Cite this article as: Li Z, Chen Y, Zhang Y, Shi J, Wan Y. Quantitative energy spectrum CT in differential diagnosis of aldosterone-producing adenoma and cortisol-producing adenoma. Quant Imaging Med Surg 2023;13(8):5012-5021. doi: 10.21037/qims-22-1279

